RANS simulation of a radial compressor for supercritical CO_2 Brayton cycle

Seong Gu Kim[a], Seong Kuk Cho[a], Jekyoung Lee[a], Jae Eun Cha[b], Si Woo Lee[c], Jeong Ik Lee[a*]
[a]*Dept. Nuclear & Quantum Eng., KAIST, 373-1, Guseong-dong, Yuseong-gu, Daejeon, 305-701, Republic of Korea*
b Korea Atomic Energy Research Insitute,150-1,Dukjin-dong, Yuseong-gu, Daejeon, 305-353, Republic of Korea
[c]*Jinsol Turbo, 305-509, Gwanpyeong-dong 695, Yuseong-gu, Daejeon, Republic of Korea*

**Corresponding author : jeongiklee@kaist.ac.kr*

1. Introduction

The supercritical CO_2 Brayton cycle (S-CO_2 cycle) is considered as one of the most promising candidates for various heat sources because it has higher cycle efficiency than the other closed Brayton cycles. Furthermore, S-CO_2 cycle has a small footprint due to the compact turbomachine and heat exchanger. It was found that the S-CO_2 compressor consumes small compression work if the operating conditions approach to the critical point (7.38MPa, 31.1℃). Therefore, this reduced compression work contributes to high cycle efficiency. Due to the above mentioned advantages, the S-CO_2 cycle can be applied to various heat sources such as coal power, bottoming cycle of fuel cells, and the next generation nuclear systems.

To demonstrate the S-CO_2 cycle performance, an integral test facility is necessary. Therefore, the joint research team of KAERI, KAIST, POSTECH designed a supercritical CO_2 integral experiment loop (SCIEL). The experimental data from this loop are accumulating in various conditions, rotational speed. The facility achieved stable compressor operation up to 35,000 rpm under supercritical CO_2 condition. The design of a S-CO_2 compressor operating near the critical point is one of the major technical challenges in the development of cycle components. The twin impeller type compressor was designed to cancel out its axial loading. The flow is divided into two lines, and enters either side of the compressor inlet. [1] The design & manufacture of compressor was conducted by Jinsol Turbo.

RANS (Reynolds-Averaged Navier Stokes equations) simulation with two-layer k-epsilon turbulence model was applied to predict the manufacture and tested S-CO_2 compressor performance [2]. Also, the obtained result was compared to the experimental result from the SCIEL facility. Until now, the design methodology of turbomachinery was not fully established. Thus, the development for loss models with S-CO_2 fluid is necessary. Detail internal flow information inside the turbomachinery can be obtained from 3-D CFD analysis. Therefore, the compressor loss models can be validated and founded. In this paper, the authors present a CFD method for a radial compressor with accurate supercritical CO_2 properties.

2. Analysis model

A commercial CFD code, Star-CCM+ V10.06 was used for the CFD analysis. [3] The entire compressor geometry including volute case, outlet diffuser was converted to the fluid domain. The geometry of the compressor is shown in Fig. 1. The fluid domain was divided into stator and rotor parts. The interface region was connected by mixing-plane approach. Two-layer k-epsilon turbulence model was used. Pressure, temperature boundary condition obtained from experiment was used for inlet, outlet condition.

Fig. 1. Geometry of SCIEL compressor.

For the property implementation of supercritical CO_2, CSV table (A database file format) was made from a simple MATLAB code. The CO_2 properties were read from the NIST Refprop 8.0 database. The relative errors of properties are shown in Table 1. The table contains density(P,T), dynamic viscosity(P,T), enthalpy(P,T), entropy(P,T), speed of sound(P,T), and thermal conductivity(P,T). The table mainly used for simulation has ranges of 0.1-20MPa, 253-2000K with 1,000 by 1,000 resolution.

Table 1. Property errors with 1,000 by 1,000 CSV table.

313.77K, 7.929MPa			
	Star-CCM+	NIST Refprop	Error
Density	264.97	264.51	**0.174%**
Enthalpy	408.21	408.37	**0.039%**
Entropy	1.6756	1.6761	**0.030%**
Thermal conductivity	40.023	39.886	**0.343%**
Dynamic viscosity	2.1818e-05	2.1796e-05	**0.101%**

To obtain an initial converged solution, the constant properties assumption was employed. After that, the property was changed from constant to CSV table, and converged solution with accurate S-CO_2 property was obtained. The convergence criteria are summarized in Table 2.

The polyhedral mesh with 8 prism layers was generated in the Star-CCM+. The growth ratio of the layers was 1.3. The mesh mainly used in this study composed of 606,201 cells. To activate high y+ wall treatment with wall function, the y+ value of the cell near the wall was 30< y+ <300. Fig. 2. shows the mesh shape used in this study.

Table 2. Convergence criterion.

	Residual
Continuity	1.0e-05
Momentum	1.0e-08
Energy	1.0e-10
Turbulent kinetic energy	1.0e-12
Turbulent dissipation rate	1.0e-20

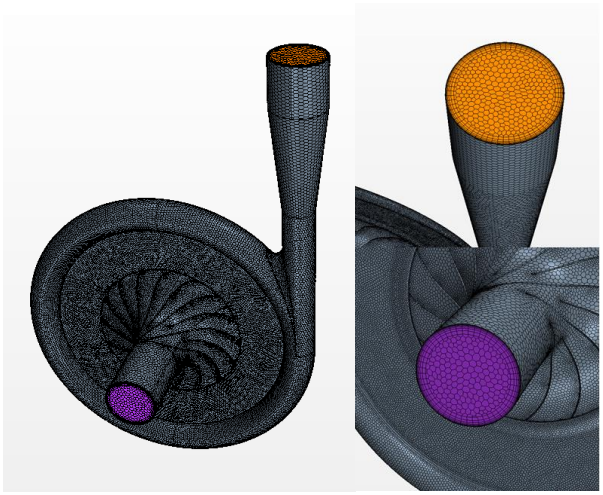

Fig. 2. Mesh shape of compressor.

3. Setup conditions

The inlet condition of 7.8-7.9MPa, 40-42℃ and various outlet conditions from the experiment were applied. The rotational speed of impeller part was 35,000rpm. At the given inlet and outlet conditions, mass flow rate and torque on the impeller surface were calculated as the output variables. After the solver obtains converged solution, target mass flow option was applied to set the mass flow rate as an outlet boundary condition. As a result, outlet temperature and mass flow rate were calculated under this target mass flow rate conditions.

The original design condition of the compressor is 1.8 pressure ratio at 75,000rpm. However, experiment did not reach this point yet due to the bearing limit. The main on-design variables of compressor are shown in the Table 3.

The residuals of mass, momentum, and energy, and turbulent kinetic energy, turbulent dissipation rate were observed. In addition, mass flow rate and temperature at outlet surface were observed to know whether the current iteration reached a converged solution or not.

Table 3. Design variables of compressor.

Design variable	Compressor
Total inlet temperature	33℃
Total inlet pressure	7.8MPa
Pressure ratio	1.8
Mass flow rate	3.2kg/s
Total to total efficiency	65%
Number of vanes	16
Shaft speed	75,000rpm

4. Performance result

Numerical and experimental results were converted to the non-dimensional variables for performance characteristic: (1) flow coefficient, (2) Pressure ratio (Total), (3) Total-to-total efficiency.

$$\phi = \frac{Q}{ND^3} \quad \text{- - - (1)}$$

$$P = \frac{P_{02}}{P_{01}} \quad \text{- - - (2)}$$

$$\eta = \frac{\dot{m}(h_{02s} - h_{01})}{T\omega} \quad \text{- - - (3)}$$

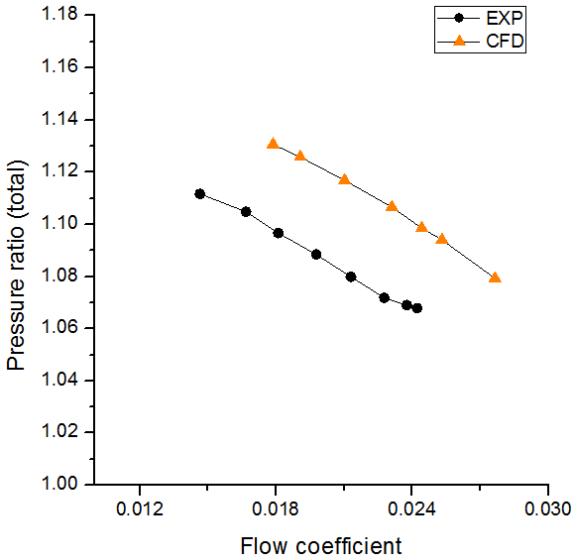

Fig. 3. Comparison of pressure ratio versus flow coefficient.

As shown in Fig. 3, CFD results showed similar characteristic when compared to experimental results. However, the numerical results showed little higher outlet pressure than that of the experiment's. It is seemed that the lower flow resistance in the CFD domain results in higher flow coefficient. In the CFD analysis, additional bypass flow through the forward surface and backward disk were not included. If an

analysis includes front and backward disk friction and rotor shaft, the pressure ratio in CFD result will be closer to the experimental curve.

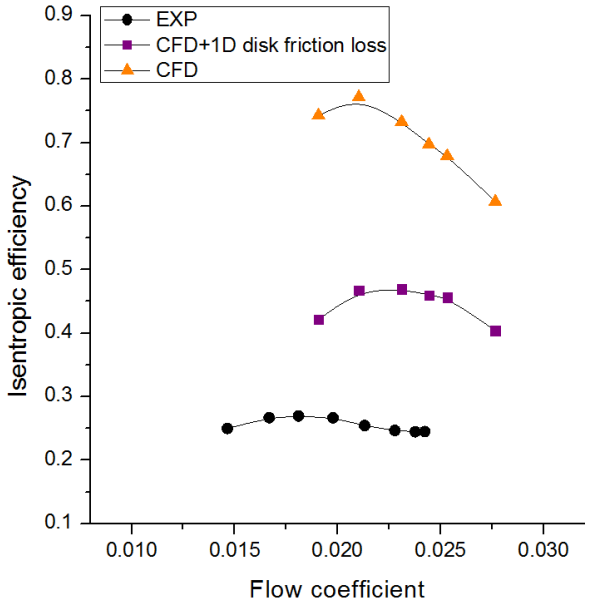

Fig. 4. Comparison of isentropic efficiency versus flow coefficient.

Fig. 4. shows isentropic efficiency results of CFD analysis and experiment. In addition, CFD result with 1-D disk friction loss was estimated. A loss model for disk friction loss was proposed by Daily and Nece [4].

$$\Delta h_{df} = f_{df} \frac{\overline{\rho} r_2^2 U_2^3}{4\dot{m}}$$

$$where\ \overline{\rho} = \frac{\rho_1 + \rho_2}{2},\ f_{df} = \frac{0.0622}{\mathrm{Re}_{df}^{0.2}},\ \mathrm{Re}_{df} \geq 3\times10^5,\ \mathrm{Re}_{df} = \frac{U_2 r_2}{\nu_2}$$

The CFD-obtained isentropic efficiency (0.60-0.77) showed large discrepancy with experimental results (0.24-0.27). The second CFD results (purple dots) are including the 1D disk friction losses on the frontward and backward faces. Yet, this result showed higher than the experimental result. The remaining difference in efficiency is seems to related to the windage loss, and leakage loss. This analysis model excludes windage loss on the rotating shaft, leakage flow through the labyrinth seal. Therefore, further numerical results with local analysis model for above loss mechanisms required to understand the large discrepancy.

The contour plot results were displayed to see the internal flow field. This result was obtained in the off-design point at 35,000 rpm. Fig. 5 shows the velocity vector in the impeller domain, and Fig. 6. shows the pressure distribution inside the impeller. The minimum pressure at the leading edge is 7.697MPa, which maintains its supercritical state.

5. Conclusions

A radial compressor geometry designed for supercritical CO_2 loop was utilized for CFD analysis. The preliminary results were compared to the experimental data. In this study, the authors present a CFD approach with accurate CSV type property table. Compared results showed reasonable difference in pressure ratio between CFD and experiment. However, additional local model analysis and 1-D loss model corrections are required to account for discrepancy in efficiency. In further works, the loss models used for the design of S-CO_2 compressor will be validated, and established with CFD results.

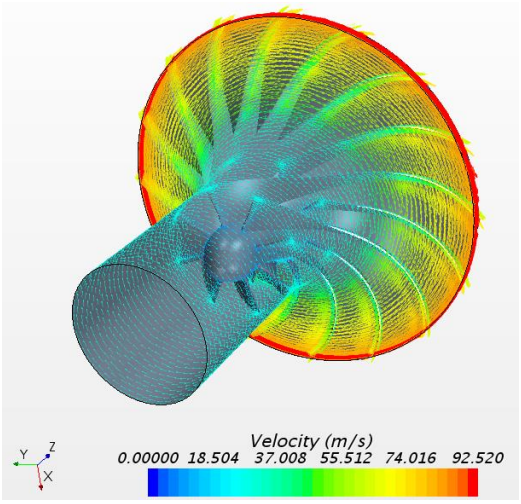

Fig. 5. Velocity vectors inside the compressor.

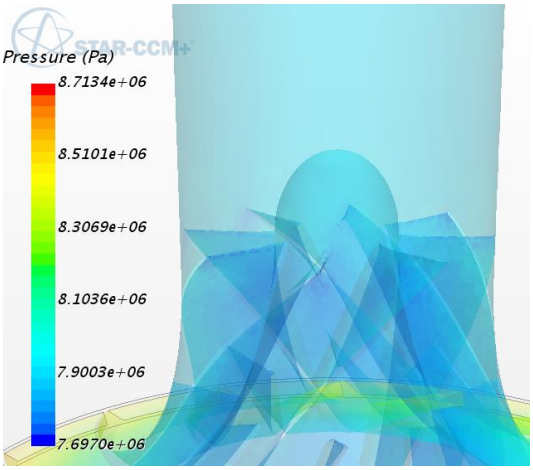

Fig. 6. Pressure distribution inside the compressor.

ACKNOWLEDGEMENT

Authors gratefully acknowledge that this work was supported by the National Research Foundation of Korea (NRF) grant funded by the Korea government (MSIP)

REFERENCES

[1] Jae Eun Cha, Seong Won Bae, Jekyoung Lee, Seong Kuk Cho, Jeong Ik Lee, Joo Hyun Park, Operation Results of a Closed Supercritical Simple Braycon Cycle,

The 5th International Symposium-Supercritical CO2 Power Cycles, March 28-31, 2016, San Antonio, Texas.

[2] Rodi, W., Experience with two-layer models combining the k-epsilon model with a one-equation model near the wall, AIAA, Aerospace Science Meeting, 29th, Reno, NV, Jan. 7-10, 1991, 13p.

[3] CD-adapco, Star-CCM+ V9.02 User Guide, 2014.

[4] Daily, J. W. and Nece, R. E. Chamber dimension effects on induced flow and frictional resistance of enclosed rotating disks. Trans. ASME, J. Basic Engng, 1960, 82, 217-232.